Petroleum Research 11 (2026) 92–100

Contents lists available at ScienceDirect

Petroleum Research

journal homepage: http://www.keaipublishing.com/en/journals/petroleum-research/

Full Length Article

Synthesis and examination of graphene oxide grafted with copolymer of maleic acid and acrylic acid as a clay stabilizer for enhancing oil production

Momodou A. Jallow [b], Abeer Alarawi [a], Tawfik A. Saleh [b,*]

[a] Production Technology Division, Saudi Aramco, Dhahran 31311, Saudi Arabia
[b] Chemistry Department, King Fahd University of Petroleum and Minerals, Dhahran 31261, Saudi Arabia

ARTICLE INFO

Article history:
Received 12 November 2024
Received in revised form
25 September 2025
Accepted 25 September 2025
Available online 26 September 2025

Keywords:
Sodium bentonite
Hydration
Oil production operation
Clay stabilizer fluids
Hydration inhibition fluid

ABSTRACT

In oil and gas production operations, wellbore instability is primarily caused by shale hydration. Thus, a thermally stable inhibitor is essential to prevent shale hydration. This research focuses on synthesizing a copolymer of maleic acid and acrylic acid/graphene oxide (poly-(AAMA)-GO) via free radical polymerization as an effective and low-cost inhibitor. The combination of the copolymer and graphene oxide aims to produce a fluid inhibitor with high thermal stability. Additionally, the unmodified copolymer of acrylic acid and maleic acid poly-(AAMA) was synthesized for comparative analysis. The inhibitory properties of both compounds were evaluated using anti-swelling, immersion, and shale recovery tests, with potassium chloride (KCl) serving as the industry benchmark. Poly-(AAMA) and poly-(AAMA)-GO effectively inhibited sodium bentonite swelling, achieving anti-swelling ratios of 75% and 78%, respectively, compared to 58% for KCl. Characterization revealed that poly-(AAMA) and poly-(AAMA)-GO adhered to sodium bentonite particles through electrostatic interactions and hydrogen bonding, forming a thin film that enhanced hydrophobicity and limited water penetration into the interlayers. Poly-(AAMA)-GO exhibited excellent thermal stability up to 250 °C, demonstrating its potential for high-temperature well fluid. Despite their structural differences, both compounds exhibited similar inhibitory effectiveness due to their shared chemical characteristics.

© 2025 Chinese Petroleum Society. Publishing services by Elsevier B.V. on behalf of KeAi Communications Co. Ltd. This is an open access article under the CC BY-NC-ND license (http://creativecommons.org/licenses/by-nc-nd/4.0/).

1. Introduction

The effectiveness of clay hydration inhibitors plays a critical role in ensuring the success and efficiency of production operations. During production, water-sensitive clay minerals can swell or disperse upon contact with aqueous fluids, leading to formation damage, wellbore instability, reduced permeability, and flow restriction. By preventing clay swelling and dispersion, these inhibitors help maintain the integrity of the reservoir and production pathways. This translates to improved well productivity, reduced downtime, lower maintenance costs, and extended equipment life. Therefore, optimizing the selection and concentration of clay hydration inhibitors is vital for maintaining operational continuity and enhancing hydrocarbon recovery (Ma et al., 2021b, 2022; Saleh, 2022a,b). Different fluids are used depending on the oil production conditions. Generally, fluids are considered more efficient in shale areas because they do not hydrate the clay content in shale. However, they have drawbacks, including high cost, environmental concerns, and limited logging capabilities, which hinder compliance with stringent environmental regulations and cost-control standards (Li et al., 2018; Zhang et al., 2019a,b). Consequently, fluids are increasingly being replaced by chemicals, which are more cost-effective and environmentally friendly (Jallow et al., 2025).

When fluids are used, shale is prone to hydration and dispersion problems. Prolonged contact between the formation and fluids exacerbates shale hydration (Bai et al., 2023; Zhou et al., 2023). Shale formations, which account for more than 70% of formations, are responsible for most wellbore stability issues. These issues include reductions in wellbore diameter, collapses, stuck pipes, and even disruptions to operations (Chen et al., 2024;

* Corresponding author.
E-mail addresses: tawfikas@hotmail.com, tawfik@kfupm.edu.sa (T.A. Saleh).
Peer review under the responsibility of Editorial Office of Petroleum Research.

https://doi.org/10.1016/j.ptlrs.2025.09.003
2096-2495/© 2025 Chinese Petroleum Society. Publishing services by Elsevier B.V. on behalf of KeAi Communications Co. Ltd. This is an open access article under the CC BY-NC-ND license (http://creativecommons.org/licenses/by-nc-nd/4.0/).

Xu et al., 2023a, 2023b). Studies have shown that expansions in clay volume and interlayer spacing are the primary internal factors that reduce rock strength and indentation hardness. This reduction directly compromises cementation strength (Liu et al., 2014; Ma et al., 2021a,b).

Developing effective shale inhibitors requires an understanding of how shale swells when fluids are used. Due to their high clay mineral content, including montmorillonite, water readily infiltrates shale formations, leading to significant swelling (Wei et al., 2023). In clay lattices, isomorphic substitution of metal atoms generates negative charges that are largely balanced by exchangeable cations in the interlayers. Clay minerals hydrate via two mechanisms: crystalline hydration and osmotic hydration. In crystalline hydration, water molecules are directly adsorbed onto the crystal surface, resulting in short-range swelling. In contrast, osmotic hydration occurs when water molecules diffuse into the interlayers, if the cation concentration differs from that of the surrounding water, resulting in extensive swelling (Jiang et al., 2019; Saleh et al., 2023).

The industry is increasingly interested in shale inhibitors that combine effective performance with environmental benefits. One widely used inhibitor is KCl (Boruah et al., 2024). In montmorillonite, the exchange of sodium ions (Na^+) with weakly hydrated potassium ions (K^+) inhibits hydration (Yang et al., 2019). However, certain offshore locations reject KCl due to its high dosage requirement (Ao et al., 2024). While high electrolyte concentrations can prevent hydration and swelling in water-sensitive shale, they also cause flocculation of clay minerals in the fluid. This flocculation adversely affects fluid properties, resulting in loss of fluid volume and reduced thixotropy, and further impairs the rheological performance of bentonite-based fluids, especially in marine environments (Sudharsan and Khare, 2023). Various chemical agents have been employed to address shale instability, including silicates, organic amines, surfactants, asphalts, polymer/KCl composites, and nanoparticles (Dai et al., 2024; Fakhari et al., 2023; Jain et al., 2017; Li et al., 2023).

Polymers, on the other hand, enhance production operation by controlling viscosity, improving suspension stability, and inhibiting shale formation while also enhancing filtration characteristics (Feng et al., 2019; Xu et al., 2023). Hydrogen bonding between the water/polymer system and the shale matrix plays a key role in shale inhibition. Because the shale matrix strongly adsorbs water, it is prone to swelling and dispersion; polymers disrupt the hydrogen bonds between water molecules and clay minerals by competing for interlayer spaces and forming bonds with aluminates and silicates. This interaction further inhibits shale hydration (Du et al., 2020). However, the high temperatures and salinity encountered during production operation can compromise polymer stability, which in turn affects overall fluid performance. Thus, modifying polymers to withstand harsh conditions is crucial (Bai et al., 2024; Dong et al., 2022). Studies have demonstrated that graphene oxide possesses excellent inhibitory properties due to its thermal and mechanical stability. Its high surface area enables the formation of a protective layer on shale surfaces, preventing water penetration (Li et al., 2024). Additionally, graphene can enhance wellbore stability by filling microspores and fractures in the shale, thereby blocking water intrusion (Saleh and Nur, 2023). A significant drawback, however, is graphene's poor dispersibility in fluids.

While KCl reduces shale hydration by exchanging potassium ions with sodium in the clay interlayers, this effect is temporary and reversible. Moreover, KCl does not form a persistent barrier against water ingress, and high ionic concentrations can cause osmotic swelling in certain clays. Additionally, its high salt load raises environmental concerns due to disposal issues in sensitive ecosystems. Conventional polymer-based inhibitors, such as polyacrylamides and polyanions, rely on adsorption onto clay surfaces to block hydration. Under high-temperature downhole conditions (>150 °C), polymer chains undergo thermo-oxidative degradation and chain scission, leading to molecular weight reduction and loss of adsorption capability. This weakens film-forming ability and results in poor long-term inhibition.

Our Approach, the design of a composite of acrylic acid, maleic acid, and graphene oxide designated as poly-(AAMA)-GO directly addresses these issues. The maleic acid–acrylic acid backbone provides strong hydrogen bonding and electrostatic adsorption sites, while graphene oxide contributes a thermally stable, high-surface-area framework that resists aggregation through covalent grafting. This dual mechanism improves coating persistence and inhibition efficiency even at 250 °C, exceeding the stability limits of many conventional inhibitors. This polymer was synthesized using free radical polymerization of acrylic acid, maleic acid, and graphene oxide. The synthesized inhibitor exhibits electrostatic interactions and hydrogen bonding, making it well suited for inhibiting shale hydration in water-based mud. For comparison, the unmodified copolymer, poly (acrylic acid-*co*-maleic acid) (poly-(AAMA)), was also synthesized, and its inhibitory properties were evaluated against those of the polymer–graphene oxide composite. The performance of both inhibitors was assessed using shale recovery, anti-swelling, and immersion tests, with KCl serving as the industry benchmark.

2. Experimental

2.1. Chemicals

Sodium bentonite (Na-Bt) 100% pure was purchased from Belle Chemical, and Maleic acid (MA) ($C_4H_6O_5$, M $r = 134.09$ g/mol, 99 % purity) was obtained from Fluka Chemie AG, Industriestrasse. Ammonium persulfate (APS) ($(NH_4)_2S_2O_8$, Mr = 228.18 g/mol, ≥98 % purity) and Acrylic acid (AA) ($C_3H_4O_2$, $Mr = 72.063$ g/mol, 99 % purity) were purchased from Sigma-Aldrich. KCl, Mr = 74.55 g/mol, purity 99 %) used for comparison was purchased from Fisher Scientific Company. Shale cutting was provided by the geology department of KFUPM. All the utilized chemicals were of analytical grade. In all experiments, deionized water was used.

2.2. Materials preparation

The composite was prepared using free radical polymerization in aqueous media (Liang et al., 2020; Tarannum et al., 2020). A dry, three-neck, round-bottom flask (150 mL) was equipped with a reflux condenser, a nitrogen gas inlet, a magnetic stirrer, and a dropping funnel. Approximately 100 mg of graphene oxide, produced by a modified Hummers' method (Abdullahi et al., 2020), was added to 50 mL of deionized water and magnetically stirred to ensure complete dispersion. A molar ratio of 3:1 for maleic acid (MA) to acrylic acid (AA) was selected, with 3 g of MA and 0.62 g of AA added to the flask. The temperature was raised to 60 °C under magnetic stirring, dissolving the components to yield a homogeneous solution. Once the reactants were completely dissolved, approximately 5 mg of APS was added in batches. The mixture was maintained under reflux for 5 h, after which three times the volume of absolute ethanol was added to precipitate the macromolecular product. The resulting product was dialyzed against deionized water to remove unreacted monomers and subsequently freeze-dried to eliminate the solvent. The collected copolymer of acrylic acid, maleic acid, and graphene oxide composite weighed 2.3 g and was designated as poly-(AAMA)-GO. The same method was used to synthesize poly-(AAMA) without graphene oxide (see Fig. 1).

2.3. Characterization and mechanism analysis tests

2.3.1. Proton- Nuclear Magnetic Resonance spectroscopy (H-NMR) analysis

A 600 MHz JEOL spectrometer was used to acquire proton Nuclear Magnetic Resonance (^{1}H-NMR) data for the monomers in solution and for poly-(AAMA). Individual NMR tubes were prepared with each sample dissolved in deuterium oxide (D_2O) at room temperature.

2.3.2. Fourier-transform infrared spectroscopy (FTIR)

For FTIR analysis, 200 mg of KBr and 2 mg of sample were thoroughly mixed and pressed into a pellet under 3 MPa using a hydraulic press. A Nicolet iS10 FTIR spectrometer was used to record the spectra of poly-(AAMA)-GO, poly-(AAMA), pristine Na-Bt, and modified Na-Bt samples.

2.3.3. Thermogravimetric analysis (TGA)

Five grams of Na-Bt were added to a beaker containing 100 mL of distilled water with a 4% inhibitor. The mixture was magnetically stirred for 24 h to ensure maximum absorption. TGA analyses were performed using a STARe System TGA/DSC 3+ machine under a high-purity Ar atmosphere at a heating rate of 10 °C/min on pristine Na-Bt, poly-(AAMA)-modified Na-Bt, and poly-(AAMA)-GO-modified Na-Bt samples.

2.3.4. Contact angle test

Three grams of Na-Bt were added to 100 mL measuring cylinders containing either distilled water, a 10% (w/w) KCl solution, or a 4% (w/w) inhibitor solution. The dispersions were stirred for 24 h to reach adsorption equilibrium. The samples were then filtered and dried at 90 °C, and the resulting residues were pressed under 5 MPa to form pellets with smooth surfaces. A droplet of distilled water was deposited on the surface of each pellet using a micro-injector attached to a Kruss Goniometer DSA25, and images were captured to determine the contact angle.

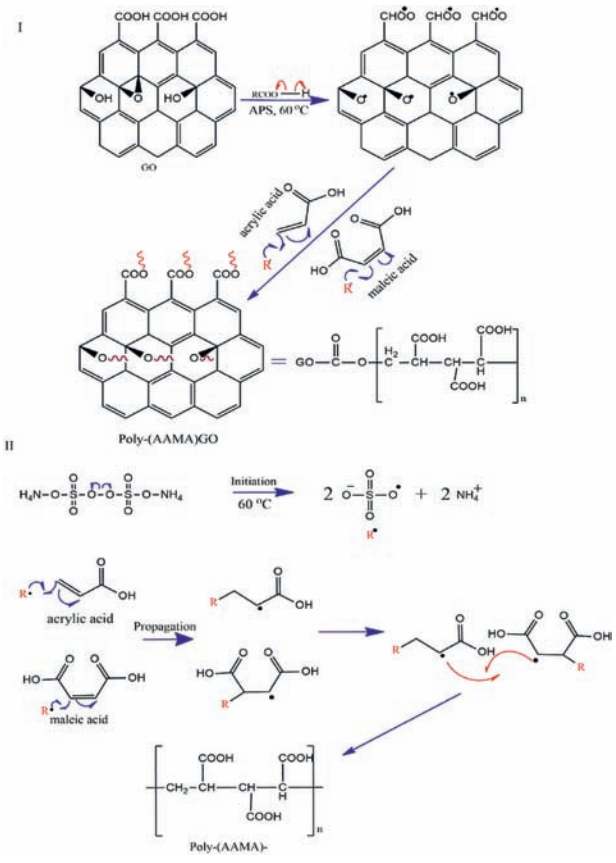


Fig. 1. A scheme illustrating the reaction of free radical polymerization of the copolymer of acrylic acid and maleic acid/graphene oxide (poly-(AAMA)GO) (I) and free radical polymerization of acrylic acid and maleic acid (II).

2.3.5. Scanning electron microscopy (SEM)

In three separate beakers, 5 g of Na-Bt was added along with 100 mL of distilled water or 100 mL of a 4% inhibitor solution to form slurries. The mixtures were stirred for 24 h to reach equilibrium absorption, then filtered. The residues were dried in an oven, mounted on tape, and coated with a thin gold layer. The morphology of samples treated with distilled water and those treated with the inhibitor solution was compared using a Thermo Scientific™ Quattro ESEM operating in high-vacuum mode.

2.3.6. X-ray diffraction (XRD)

XRD patterns of pristine sodium Na-Bt in distilled water and Na-Bt soaked in a 4% inhibitor solution were recorded using an Ultima IV X-Ray diffractometer with a copper target. The 2θ scanning range was 30°–100°. For sample preparation, 5 g of Na-Bt was mixed with either 100 mL of distilled water or 100 mL of a 4% inhibitor solution, stirred for 24 h to form a slurry, filtered, dried at 60 °C, and ground into powder. The d_{001} spacing was calculated using Bragg's equation: $2d \sin\theta = n\lambda$.

2.4. Performance evaluation tests

2.4.1. Shale recovery test

An inhibitor solution was prepared and mixed with shale cuttings in a pressurized, sealed vessel to determine the degree of dispersion. A higher recovery percentage indicates a better ability to prevent shale dispersion. Approximately 5 g of shale cuttings (6–10 mesh) were placed in sealed vessels containing 35 mL of either distilled water, a 10% KCl solution, or a 4% inhibitor solution. The sealed vessels were then placed in a roller oven and hot-rolled at 120 °C for 16 h. Afterward, the mud was washed with deionized water, filtered, and dried at 110 °C. The recovery percentage was calculated as:

$$Recovery = \frac{M_2}{M_1} x\ 100$$

where M_2 is the mass of shale cuttings after hot rolling and M_1 is the initial mass before hot rolling.

2.4.2. Plate soaking test

Pallets were prepared by pressing 5 g of Na-Bt under 10 MPa for 5 min using a hydraulic press. The compacted Na-Bt pallets were then immersed in Petri dishes containing 25 mL of distilled water, 25 mL of a 10% KCl solution, or 25 mL of a 4% inhibitor solution. The samples were maintained at room temperature for two days, and photographs were captured at 5 min, 30 min, 1 h, 3 h, 7 h, 24 h, and 48 h to document the hydration process.

2.4.3. Anti–swelling test

As a standard method to evaluate Na-Bt clay stabilizers in fluids, the anti-swelling test assesses the influence of inhibitors on Na-Bt. One gram of Na-Bt was placed in a centrifuge tube containing 20 mL of a 4% inhibitor solution. After thorough stirring and shaking, the tubes were left undisturbed for 2 h. The mixture was then centrifuged at approximately 1500 rpm for 15 min, and the change in Na-Bt volume was measured. The anti-swelling ratio (AR) was calculated using the equation:

$$AR = \frac{V_b - V_a}{V_b - V_o} x\ 100$$

where V_a is the volume of Na-Bt in the inhibitor solution, V_b is the volume in water, and V_o is the volume change measured with kerosene.

3. Results and discussion

3.1. Characterization of GO, Poly-(AAMA) and Poly-(AAMA)GO

3.1.1. Nuclear Magnetic Resonance (NMR)

The structure of the resultant product was characterized using H-NMR spectroscopy. As shown in Fig. 2 for poly-(AAMA): the peak at 2.9 ppm can be attributed to 3H, of CH; whereas that of 1.4 ppm for 2H, of CH_2; the H of –COOH does not exhibit a signal in the D_2O solvent, and the peak at 4.70 ppm is ascribed to the solvent (D_2O). Notably, the spectrum indicates no transmittance for the C=C peak at 5.5–6.2 ppm, providing evidence for the polymerization of the monomers (Abdullahi et al., 2020).

3.1.2. Fourier transform infrared spectroscopy (FT-IR)

In order to determine the functional groups of GO, poly-(AAMA), and poly-(AAMA), FT-IR was utilized as shown in Fig. 3. In the GO FT-IR spectrum, 1721 cm^{-1} is ascribed to C=O stretching vibrations, and 1648 cm^{-1} is the absorption band for un-oxidized C=C. The bands at 3200 cm^{-1} and 1288 cm^{-1} were ascribed to the stretching vibration of –OH and C–O–C, respectively (Li et al., 2024). In the FT-IR spectrum of poly-(AAMA), the transmittance bands of carboxyl carbonyl groups and hydroxyl groups are observed at 1707 cm^{-1} and 3300 cm^{-1}. The disappearance of the transmittance band corresponding to C=C stretching vibrations (typically observed at 1645–1620 cm^{-1}) confirms the successful polymerization of the monomers, indicating that the vinyl double bonds have been consumed during the reaction. The FT-IR spectra of poly-(AAMA) and poly-(AAMA)/GO composites appear largely similar, which can be attributed to the relatively low loading of GO in the composite, making its characteristic peaks less pronounced in the overall spectrum. However, a noticeable shift of the C=O stretching band toward lower wavenumbers is observed in the composite. This shift is consistent with the formation of hydrogen bonds between the oxygen-containing functional groups of GO (such as hydroxyl, epoxy, and carboxyl groups) and the carbonyl groups of the poly-(AAMA) matrix. Such hydrogen bonding interactions provide evidence for successful interfacial compatibility and physical interactions between GO sheets and the polymer chains.

3.1.3. Thermogravimetric analysis (TGA)

Inorganic inhibitors are recognized for their high thermal stability, whereas organic inhibitors, especially polymers, tend to degrade at high temperatures (Yang et al., 2019). Hence, it is important to determine the thermal stability of inhibitors. Fig. 4 shows the thermal decomposition of poly-(AAMA) and poly-(AAMA)-GO. Poly-(AAMA) begins to decompose at around 150 °C, whereas poly-(AAMA)-GO starts decomposing above 225 °C, indicating better thermal stability. The improved thermal stability of poly-(AAMA)-GO is primarily due to the GO content.

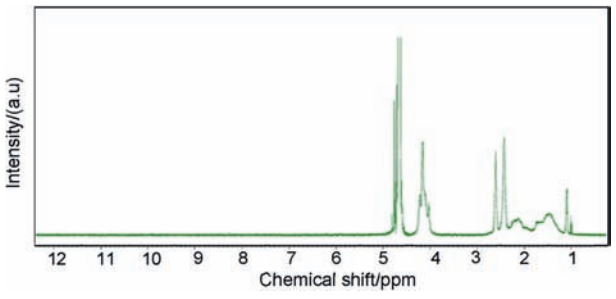


Fig. 2. The NMR spectrum of Poly-(AAMA).

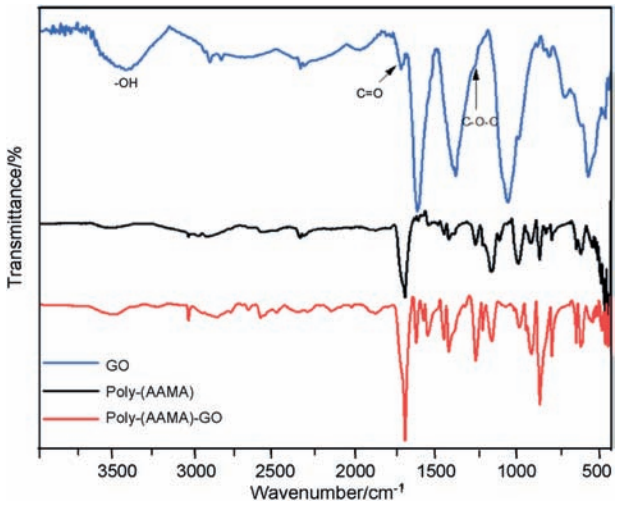


Fig. 3. The FT-IR spectrum of GO, Poly-(AAMA), and Poly-(AAMA)-GO.

3.2. Evaluation of the inhibition performance

3.2.1. Plate soaking test

When fluids enter the shale formations, the wellbore can become unstable, resulting in the collapse of the wellbore. During the plate soaking test, Na-Bt Pallets are exposed to different solutions to simulate free hydration and swelling in the downhole (Dong et al., 2022). As shown in Fig. 5, the letters a-d represent pallets in different inhibitor solutions at a time interval of 48 h. Fig. 5(a) shows the Na-Bt palate in distilled water. As it is observed, the palate shows great swelling, resulting in the palate disintegrating. Fig. 5(b) shows a palate in KCl solution in which the palate disintegrated, but there was no swelling. This is proof of KCl being an inhibitor. Fig. 5(c) and (d) show pallets in the polymer solution and polymer graphene oxide composite solution. It was seen that after 48 h of soaking, the pallets did not disintegrate and no swelling occurred, proving that the synthesized compounds are good hydration inhibitors. Inhibiting hydration with KCl is possible, but stabilizing the pallet with poly-(AAMA) and poly-(AAMA)-GO is much more effective. Based on the results of the experiment, it can be inferred that the Na-Bt pallet is less hydrated and swollen because poly-(AAMA) and poly-(AAMA)-GO have merged to its surface, preventing water from entering. Interestingly, the presence of GO has the advantage of having higher thermal stability, making it a good candidate to be used at higher temperatures.

3.2.2. Shale recovery test

Shale recovery tests are commonly used to assess the inhibitory properties of fluids in controlling cutting disintegration from the drill bit to the surface. A high-temperature dispersion of shale cuttings is mimicked by this inhibitory performance (Bai et al., 2023). The result of hot rolling in Fig. 6 indicates that the remaining shale in distilled water has a 25% shale recovery average. The shale disintegrated and displayed high dispersion,

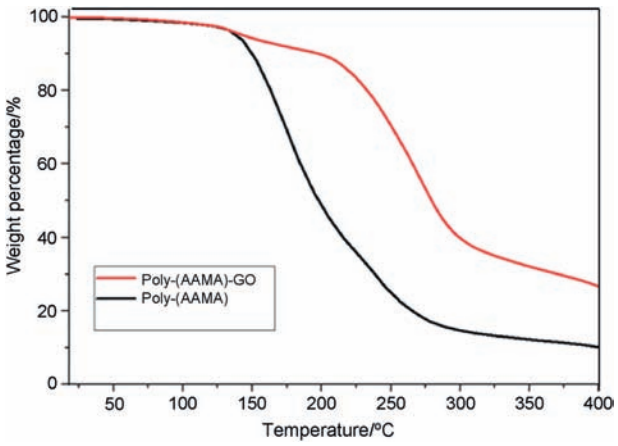


Fig. 4. TGA curves of Poly-(AAMA)-GO and Poly-(AAMA).

showing the high hydration of the shale. In comparison with the KCl solution, an increase of 30% recovery was observed in the remaining shale. The low recovery shown by KCl is a result of the weak ionic effect on shale samples. The shale recovery was further increased to an average percentage of 80% using 4% of the synthesized samples in solution. This improvement indicates that poly-(AAMA) and poly-(AAMA)-GO have a strong adsorption capacity on the cuttings of shale and can prevent hydration. The recovery of poly-(AAMA)-GO was the highest among the tested materials, which can be attributed to the presence of graphene oxide (GO) within the polymer matrix. GO nanosheets possess abundant surface functional groups and a high surface area, enabling strong interactions with rock or shale surfaces. These interactions facilitate the formation of a thin, continuous barrier layer that adheres to the surface and effectively limits water penetration into the rock matrix, thereby enhancing recovery performance.

3.2.3. Anti-swelling ratio

Analyses were carried out on Na-Bt to determine how inhibitors affected anti-swelling rate. It helps us to determine the capabilities of the inhibitor in suppressing the swelling and dispersion of the Na-Bt. In oil production operations, commonly, 10% KCl is used to inhibit swelling, which has been evaluated and compared with 4% of the inhibitors in solution. As shown in Fig. 7, poly-(AAMA) and poly-(AAMA)-GO greatly retarded the swelling of Na-Bt at an average anti-swelling ratio of 75% and 78% respectively. When compared to KCl, which shows a 58% anti-swelling ratio, the polymers and polymer graphene composite are more effective at minimizing shale hydration. The polymer interaction on the Na-Bt prevented the water molecules from infiltrating to cause significant swelling. The base copolymer poly-(AAMA) already exhibits strong inhibition due to multiple carboxyl groups capable of forming hydrogen bonds and electrostatic interactions with clay surfaces, thereby limiting water ingress into interlayers. The addition of GO, while providing additional adsorption sites and increasing surface hydrophobicity, is expected to contribute more significantly under prolonged exposure and elevated temperature–pressure conditions rather than at the 120 °C test conditions used for standard performance comparison. This explains why the performance improvement appears modest in the short-term tests but is expected to be more pronounced in harsh

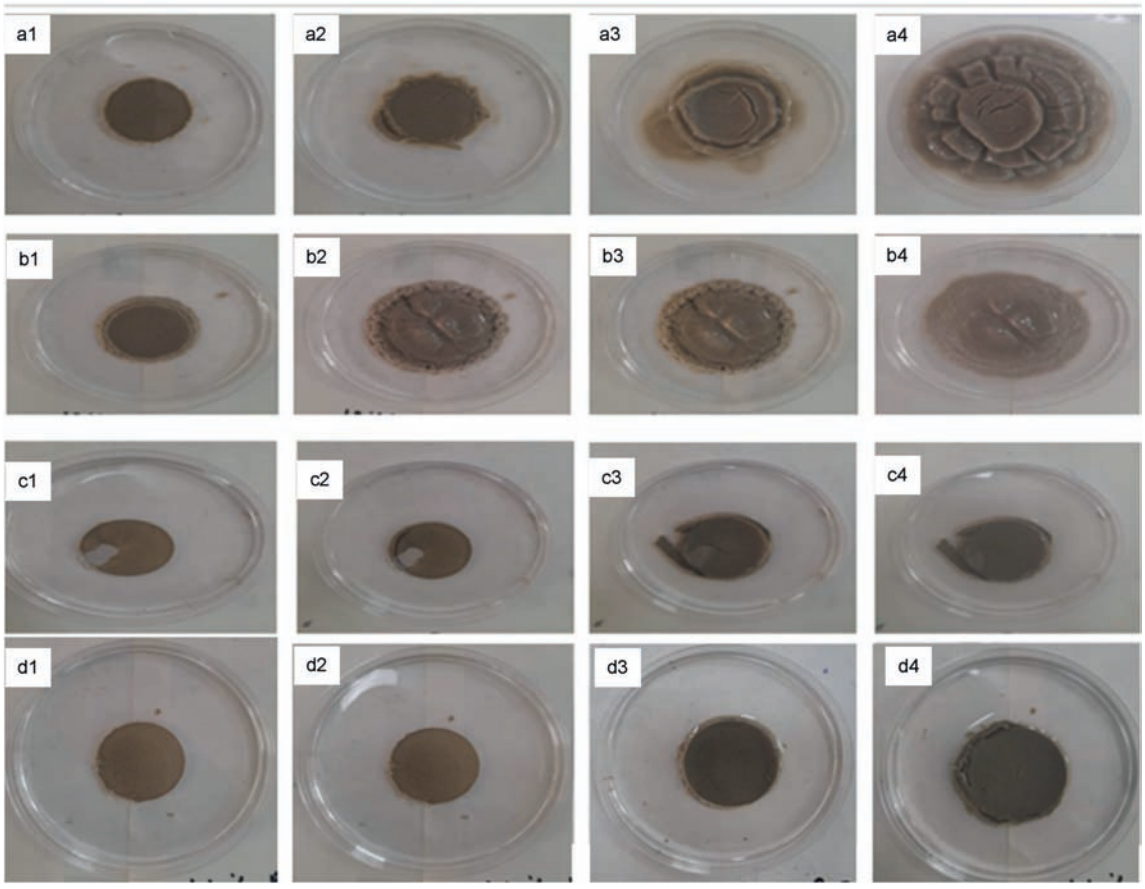


Fig. 5. Photos of Na-Bt plates soaked in the water and the various inhibitor media for 48hr: (a) water, (b) 10 wt% KCl, (c) 4 wt% poly-(AAMA), (d) 4 wt% poly-(AAMA)-GO.

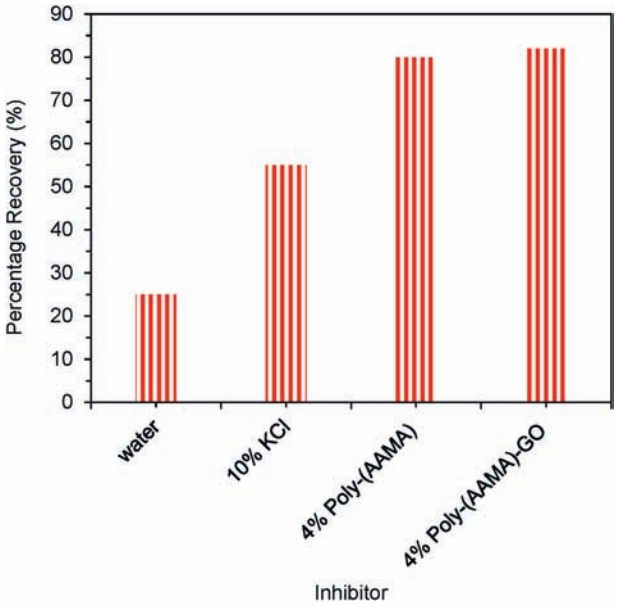


Fig. 6. The percentage recovery of the shale after hot-rolling in water and varoius inhibitor media at 120 °C for 16 h.

field conditions. In summary, GO's incorporation provides a structural and thermal reinforcement function, ensuring that the inhibitor remains stable and effective under extreme drilling conditions, even if short-term inhibition metrics at moderate temperatures show only marginal improvement.

3.3. Analysis toward proposed inhibition mechanism

3.3.1. FT-IR analysis of the inhibited clay and clay stabilizer

Fig. 8 shows the infrared spectra for the pristine Na-Bt and Na-Bt modified with poly-(AAMA) and poly-(AAMA)-GO. A typical characteristic Na-Bt group was shown by the FT-IR spectra. The following are the absorption peaks: the stretching band of Si–O–Si (469 cm-1), the deformation band of Al–O–Si (537 cm-1), the stretching band of Si–O (1030 cm-1), the water deformation band (1634 cm-1), and the stretching band –OH (3618 cm-1). For the Na-Bt modified with poly-(AAMA). There is a change in the spectra due to the absorption of the polymer into the surface. The stretching band of –OH shifted by 4 cm-1, and Si–O band shifted by 4 cm-1. Moreover, the appearance of a new peak at 1703 cm-1 indicates the stretching band of C=O, which indicates the incorporation of the polymer into the shale sample. The shifting of these common stretching bands further proves that a hydrogen bond is formed between the Na-Bt and the polymer. Furthermore, this showed that the inhibitors were well adsorbed on the Na-Bt surface. The same can be said for the sample modified with poly-(AAMA)-GO.

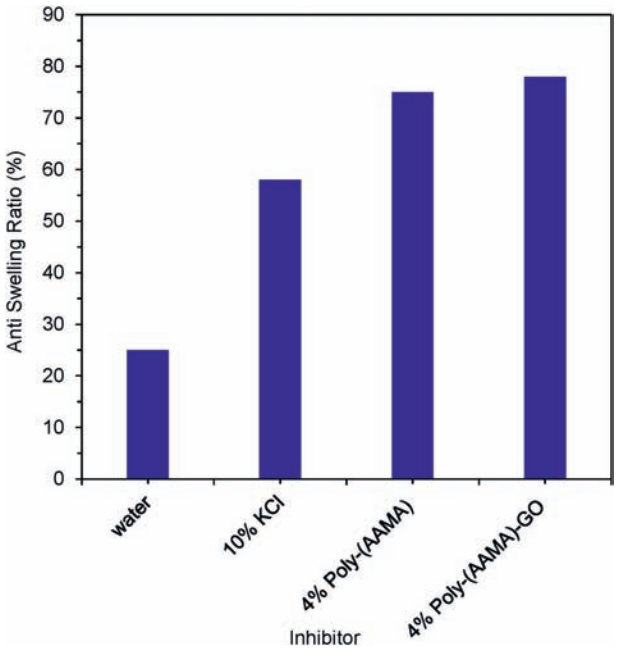


Fig. 7. Anti-swelling ratio of the prepared inhibitors compared to water and KCl.

3.3.2. SEM

Fig. 9 displays SEM images of the microscopic morphology of the pristine Na-Bt sample in water and the sample treated with 4 % poly-(AAMA) and poly-(AAMA)-GO in solution, respectively. In Fig. 9(a), the pure shale exhibits a hydrated state, evident from its porous and rough morphology, indicating Na-Bt hydration. The Na-Bt expanded and became loose when exposed to pure water. The modified Na-Bt sample in Fig. 9(b) and (c) shows more compatibility and is less porous, which is an indication of less hydration. This outcome demonstrates that the surface of the shale was covered and sealed by the inhibitor, forming a protective film on the surface of the Na-Bt, thereby preventing hydration. The SEM image in Fig. 9(c) shows a rougher surface morphology and a layered, sheet-like structure, which can be attributed to the presence of graphene. To strengthen this interpretation, EDX elemental mapping for O, and C is shown in Fig. 10. The EDX maps reveal a higher oxygen and carbon content in the composite, consistent with the oxygen-rich functional groups of graphene oxide, and a uniform distribution of C across the surface. These findings support the presence and incorporation of GO within the material and correlate with the observed morphological changes.

3.3.3. XRD analysis of the inhibited clay and clay stabilizer

XRD was used to assess changes in interlayer spacing, as this will help us to determine the hydration level of the Na-Bt when in contact with various inhibitor solutions. Fig. 11 illustrates the hydration pattern of pristine Na-Bt in water and Na-Bt in various inhibitor solutions. The diffraction peak (d_{oo1}) of the pure Na-Bt in water shows a d-value of 14.8 Å, whereas the Na-Bt samples in

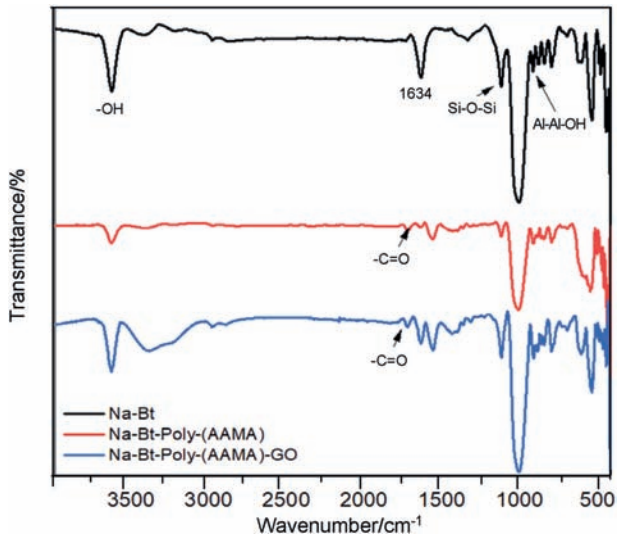


Fig. 8. FT-IR spectra of Na-Bt, Na-Bt/4% (w/v) poly-(AAMA), and Na-Bt/4% (w/v) poly-(AAMA)-GO.

inhibitor solution of poly-(AAMA) and poly-(AAMA)-GO decrease in interlayer spacing, showing a d-value of 12.1 Å and 12.2 Å, respectively. Comparing these XRD patterns indicates that the Na-Bt soak in distilled water is highly hydrated which resulting in to increase in the interlayer spacing. The decrease in the d-value of the Na-Bt in the inhibitor solution indicates less hydration, signifying that poly-(AAMA) and poly-(AAMA)-GO effectively absorbed onto the surface mineral, thereby inhibiting hydration.

3.3.4. Contact angle test

In the contact angle test, the direction of the capillary force can be determined. The high hydrophilicity indicates that capillary force drives water into the shale through spontaneous inhibition. A decrease in hydrophilicity and an increase in hydrophobicity lead to an inability of water to enter the pores in the shale, inhibiting hydration (Bai et al., 2023). The contact angles labeled a, b, c, and d in Fig. 12 are a representation of pristine Na-Bt, Na-Bt treated with KCl, and Na-Bt modified with poly-(AAMA) and poly-(AAMA)-GO. For pristine Na-Bt, an average contact angle of 19.2° was obtained, indicating the material is highly hydrophilic. The sample modified with 10% weight of KCl in solution resulted in an improved hydrophobicity, which is seen by an increase in the average contact angle to 33°. Samples C and D represent shale modifications with poly-(AAMA) and poly-(AAMA)-GO at 4% concentrations in solution. There is an increase in the sample hydrophobicity. This is evident that the synthesized material serves as a superior hydration inhibitor compared to KCl, creating a barrier that hinders water penetration into the shale samples.

3.3.5. TGA

In Na-Bt, water exists in three states: free-adsorbed water, loosely coupled water, and closely coupled water. Then, evaporation of such water states in a Na-Bt/inhibitor composite occurs in three stages: below 75 °C, 75−120 °C, and 120−230 °C. Therefore, the distribution of water in Na-Bt can be determined using TGA

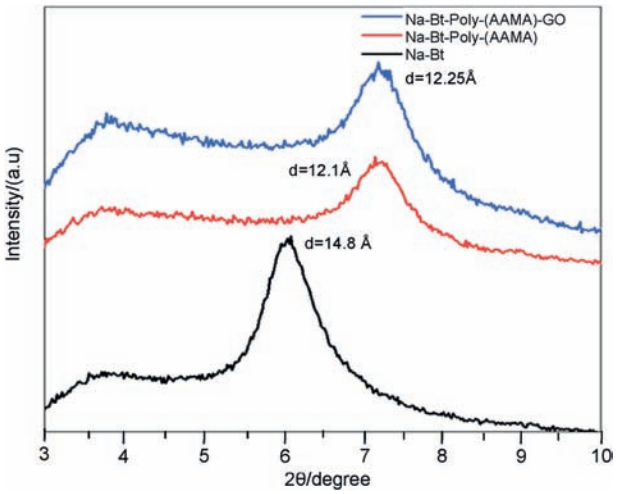


Fig. 11. The XRD plots for Na-Bt/H2O, Na-Bt/4% (w/v) poly-(AAMA), and Na-Bt/4% (w/v) poly-(AAMA)-GO.

(Yang et al., 2017). TGA can provide us with information on how much water has been absorbed by the Na-Bt. In Fig. 13, the thermal decomposition curve is shown for Na-Bt samples and Na-Bt samples modified with polymer and polymer graphene oxide. Pristine Na-Bt samples show fast decomposition as a result of dehydration of much water, and then they follow a slow decomposition pattern. The modified shale shows a very slow decomposition initially due to its small water absorption compared to the unmodified shale sample. It is evident from the gradual decomposition of modified shale that not much of the sample contains free water. Water absorption is inhibited by the polymer and polymer graphene oxide composite, proving its inhibitory properties.

3.3.6. Proposed mechanism of inhibition

Using characterization techniques, the inhibitors poly-(AAMA) and poly-(AAMA)-GO were investigated for their probable inhibitory

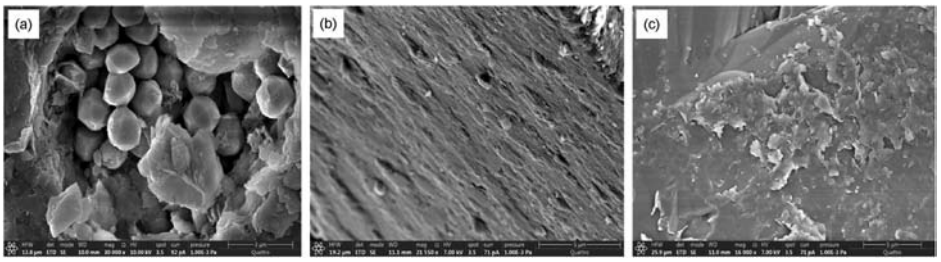


Fig. 9. SEM images for (a) Na-Bt, (b) Na-Bt/4% (w/v) poly-(AAMA), and (c) Na-Bt/4% (w/v) poly-(AAMA)-GO.

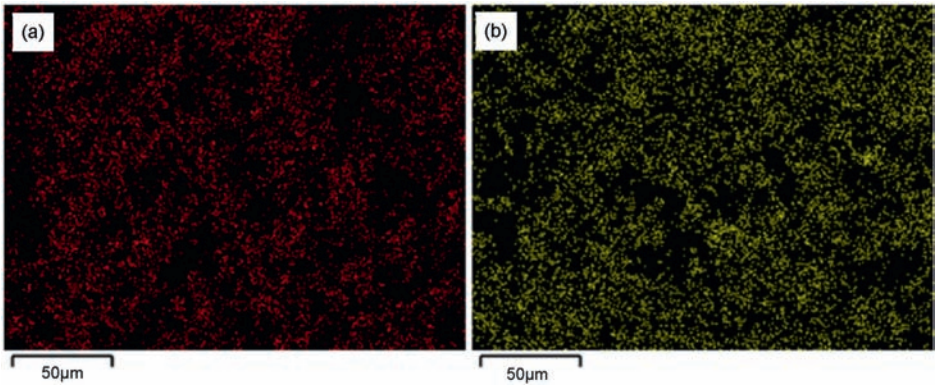


Fig. 10. EDX mapping of (a) O, and (b) C of the poly-(AAMA)-GO on the shale surface.

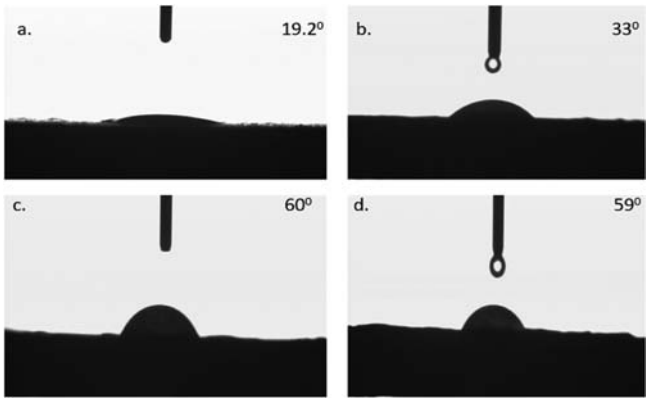


Fig. 12. Contact angle measurements of (a) pristine Na-Bt, (b) Na-Bt/10% (w/v) KCl, (c) Na-Bt/4% (w/v) poly-(AAMA), and (d) Na-Bt/4% (w/v) poly-(AAMA)-GO.

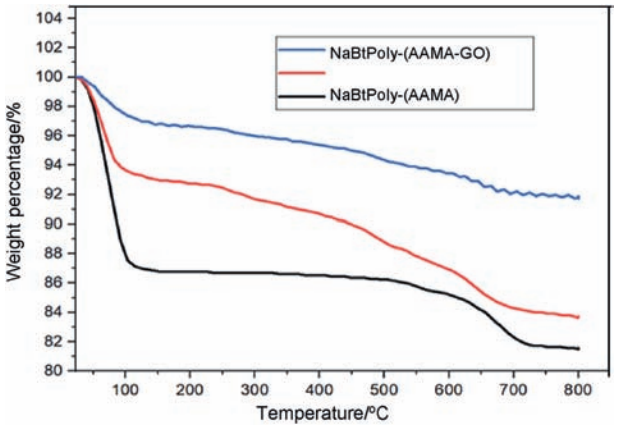


Fig. 13. The TGA plot of pristine Na-Bt, Na-Bt/4% (w/v) poly-(AAMA), and Na-Bt/4% (w/v) poly-(AAMA)-GO.

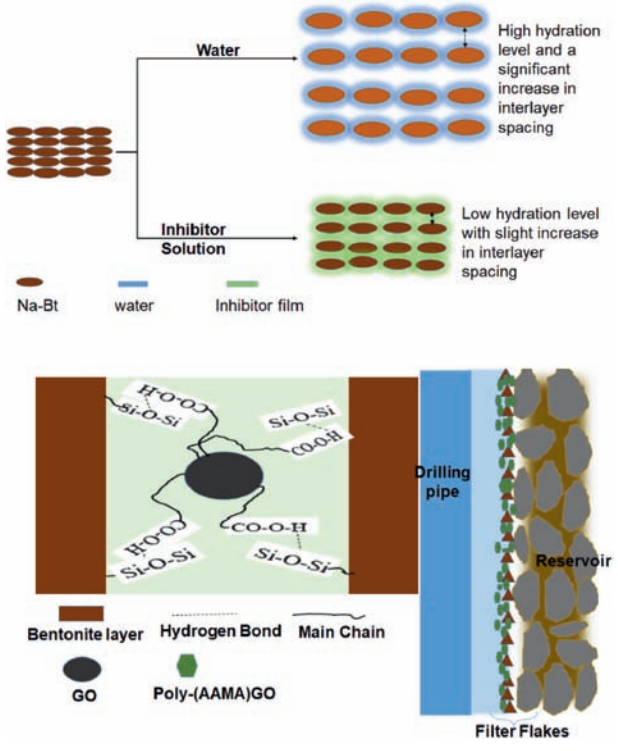


Fig. 14. The mechanism of poly-(AAMA)-GO inhibiting shale hydration swelling.

mechanism. Shale formations are seriously soaked and invaded with water due to their significant clay mineral content (Lv et al., 2020). In a clay lattice, negative charges are generated by metal atoms through isomorphic substitution, and this is compensated by the exchangeable cations in the interlayer. This results in the surface of the Na-Bt being highly hydrophilic, thus Na-Bt absorbs water and gets hydrated seriously through crystalline or osmotic hydration. The hydration of shale can be inhibited through the following approaches: chemical effects, such as electrostatic neutralization, ion exchange, and physical actions such as sealing (An et al., 2016).

For poly-(AAMA) and poly-(AAMA) -GO in solution, the many carboxyl functional groups and backbone chain of the polymers, there exist electrostatic interactions, hydrophobic interactions, and hydrogen bonds. These interactions enable the inhibitors to be easily adsorbed onto the surface of the Na-Bt and form a polymer film. As shown in Fig. 14. The polymer film forms an effective shield over the Na-Bt, thus preventing the serious soaking and intrusion of water. Thus poly-(AAMA) and poly-(AAMA) -GO act as effective inhibitors in oil production. The TGA analysis has shown that poly-(AAMA) –GO has better thermal stability than poly-(AAMA), which is due to the incorporation of GO.

These mechanisms align with established principles in polymer nanocomposites, where nanofillers such as GO improve thermal stability via barrier effects, interfacial reinforcement, and char formation. The enhanced thermal stability arises from a combination of restricted chain mobility, covalent/non-covalent interactions, barrier effects, and char-forming behavior imparted by GO. These factors collectively increase the activation energy required for thermal degradation, as evidenced by thermogravimetric analysis (TGA) data.

4. Conclusion

This study introduces a graphene oxide–reinforced acrylic acid–maleic acid copolymer (poly-(AAMA)-GO) designed specifically for high-temperature drilling applications, demonstrating stability at high temperature, a significant advancement over conventional polymer-based shale inhibitors. The incorporation of only 4% graphene oxide-based inhibitor not only enhanced the composite's thermal resilience but also maintained its inhibitory efficiency under various conditions. With an anti-swelling performance (78%) and shale recovery (80%) surpassing that of standard KCl (amounts added is 10%) treatments (58%), poly-(AAMA)-GO offers a cost-effective, thermally robust, and environmentally compatible solution for mitigating shale hydration. The inhibitor's strong adsorption via electrostatic interactions and hydrogen bonding forms a hydrophobic protective film on shale surfaces, effectively limiting water penetration even in challenging high-temperature environments. This work establishes a foundation for next-generation high-performance drilling fluid additives that combine polymer chemistry with advanced nanomaterials, opening pathways for improved wellbore stability in deep and ultra-deep reservoirs.

CRediT authorship contribution statement

Momodou A. Jallow: Methodology, Data curation, Writing - original draft. **Abeer Alarawi:** Methodology, Writing - original draft. **Tawfik A. Saleh:** Conceptualization, Validation, Data curation, Supervision.

Declaration of competing interest

The authors declare that they have no known competing financial interests or personal relationships that could have appeared to influence the work reported in this paper.

References

Abdullahi, B.O., Ahmed, E., Abdulgader, H.A., Alghunaimi, F.I., Saleh, T.A., 2020. Facile fabrication of hydrophobic alkylamine intercalated graphene oxide as absorbent for highly effective oil-water separation. J. Mol. Liq. 325, 115057.

An, Y., Yuxiu, A., Guancheng, J., Yourong, Q., Xianbin, H., He, S., 2016. High-performance shale plugging agent based on chemically modified graphene. J. Nat. Gas Sci. Eng. 32, 347–355.

Ao, H., Lin, L., Ren, R., Yang, Y., Li, X., Ren, W., Luo, P., 2024. Deep eutectic solvents with different alkyl chain lengths as inhibitors for shale in water-based drilling fluids. Energy Fuels 38 (6), 5374–5380.

Bai, J., Xiao, F., Chen, Z., Tao, L., Zhang, N., Shi, W., Zhu, Q., 2023. Investigation of the mechanism and effect of citric acid-based deep eutectic solvents inhibiting hydration and expansion of gas shale clay minerals. Energy & Fuels 37, 2750–2758.

Bai, X., Chen, Y., Wu, L., Wang, M., Luo, Y., 2024. Synthesis and properties of a novel ionic liquid copolymer shale inhibitor. J. Appl. Polym. Sci. 141 (I7), e54962.

Boruah, A., Prusty, B.K., Verma, S., 2024. Experiential investigations for shale–fluid interaction and identification of novel chemical additives as efficient shale swelling inhibitor. MRS Energy Sustain. 11, 448–459.

Chen, S., Huang, D., Xu, Z., Bai, Y., Xie, G., Li, G., Chen, H., Zhou, C., Luo, P., Feng, R., 2024. Synthesis and mechanism analysis of a non-toxic amine-based clay mineral surface hydration intercalation inhibitor. J. Mol. Liq. 399, 124362.

Dai, Z., Sun, J., Liu, J., Lv, K., Zhang, X., Wang, Z., Xu, Z., 2024. Study on the inhibition mechanism of hydration expansion of Yunnan gas shale using modified asphalt. Materials 17, 645.

Dong, T., Jiang, G., He, Y., Yang, L., Jiang, S., Yang, Y., Zhu, Y., 2022. A novel low molecular Quaternary polymer as shale hydration inhibitor. J. Mol. Liq. 370, 120934.

Du, W., Wang, X., Chen, G., Chen, G., Zhang, J., Slaný, M., 2020. Synthesis, property and mechanism analysis of a novel polyhydroxy organic amine shale hydration inhibitor. Minerals 10, 128.

Fakhari, N., Bing, C., Bennour, Z., Gholami, R., 2023. Green and biodegradable surfactant based shale inhibitors for water based fluids. J. Mol. Liq. 371, 121106, 121106.

Feng, Q., Liu, H., Peng, Z., Zheng, Y., 2019. Preparation of a cationic hyperbranched polymer for inhibiting clay hydration swelling in the process of oilfield waterflooding. Energy & Fuels 33 (12), 12202–12212.

Jain, R., Paswan, B.K., Mahto, T.K., Mahto, V., 2017. Study the effect of synthesized graft copolymer on the inhibitive water based drilling fluid system. Egypt. J. Pet. 26 (4), 875–883.

Jallow, M., Alarawi, A., Saleh, T.A., 2025. Synthesis and investigation of a graphene oxide grafted with copolymer of acrylic acid and acrylamide for shale hydration inhibition. Diam. Relat. Mater. 159 (Part A), 112721.

Jiang, G., Li, X., Zhu, H., Li, Y., Tengda, W., Xiongjun, W., 2019. Improved shale hydration inhibition with combination of gelatin and KCl or EPTAC, an environmentally friendly inhibitor for water-based drilling fluids. J. Appl. Polym. Sci. 136, 47585.

Li, T., Pang, S., Zhao, L., Yan, L., Zheng, X., An, Y., 2024. A novel graphene grated polymer as shale inhibitor in drilling fluids and study of mechanism. J. Dispersion Sci. Technol. 46 (1), 88–97.

Li, X., Jiang, G., Lili, Y., Peng, S., 2018. Study of gelatin as biodegradable shale hydration inhibitor. Colloids Surf. A Physicochem. Eng. Asp. 539, 192–200.

Li, Y., Xia, C., Liu, X., 2023. Water-based drilling fluids containing hydrophobic nanoparticles for minimizing shale hydration and formation damage. Heliyon 9 (12), e22990.

Liang, T., Yan, K., Zhao, T., Ji, B., 2020. Synthesis of a low-molecular-weight copolymer by maleic acid and acrylic acid and its application for the functional modification of cellulose. Cellulose 27, 5665–5675.

Liu, X., Liu, K., Gou, S., Liang, L., Luo, C., Guo, Q., 2014. Water-soluble acrylamide sulfonate copolymer for inhibiting shale hydration. Ind. Eng. Chem. Res. 53, 2903–2910.

Lv, K., Huang, P., Zhou, Z., Wei, X., Luo, Q., Huang, Z., Yan, H., Jia, H., 2020. Study of Janus amphiphilic graphene oxide as a high-performance shale inhibitor and its inhibition mechanism. Front. Chem. 8, 201, 201.

Ma, J., Jingyuan, M., Xia, B., Boru, X., An, Y., An, Y., Yuxiu, A., 2022. Advanced developments in low-toxic and environmentally friendly shale inhibitor: a review. J. Petrol. Sci. Eng. 208, 109578.

Ma, J., Pang, S., Zhang, Z., Xia, B., An, Y., 2021a. Experimental study on the polymer/graphene oxide composite as a fluid loss agent for water-based drilling fluids. ACS Omega 6, 9750–9763.

Ma, J., Pang, S., Zhou, W., Xia, B., An, Y., 2021b. Novel deep eutectic solvents for stabilizing clay and inhibiting shale hydration. Energy & Fuels 35, 7833–7843.

Saleh, T.A., 2022a. Experimental and analytical methods for testing inhibitors and fluids in water-based drilling environments. TrAC, Trends Anal. Chem. 149, 116543.

Saleh, T.A., 2022b. Advanced trends of shale inhibitors for enhanced properties of water-based drilling fluid. Upstream Oil Gas Technol. 8, 100069.

Saleh, T.A., Nur, M., 2023. Synthesis of polyacrylic-melamine grafted graphene as efficient inhibitor for shale stabilization in water-based drilling fluid. Mater. Today Commun. 35, 106264, 106264.

Saleh, T.A., Nur, M., Alarawi, A., 2023. Synthesis of poly (citric acid–aspartic acid) copolymer for efficient inhibition of shale hydration in water-based drilling fluids. J. Phys. Chem. Solid. 181, 111455.

Sudharsan, J., Khare, S., 2023. Pore pressure transmission test as measure of shale inhibition performance of nanoparticle additives in water based drilling fluids – a comprehensive review. Mater. Today Proc. 99, 8–14.

Tarannum, N., Suhani., Kumar, D., 2020. Synthesis, characterization and applications of copolymer of β – cyclodextrin: a review. J. Polym. Res. 27, 89.

Wei, Z., Wang, M., Shan, W., Guo, M., Li, Y., Qin, W., Li, K., An, A., Bo, K., 2023. Synergistic effects of potassium alginate and silicates co-inhibition performance in shale hydration. J. Mol. Liq. 393 (2024), 123538.

Xu, J., Luo, T., Wang, J., Zhu, S., Azadbakht, S., Lyu, X., Li, M., Wang, L., 2023. Investigation of alcohol-based deep eutectic solvents for inhibiting hydration in shale formations. J. Mol. Liq. 392 (Part 2), 123551.

Xu, J., Su, K., Meng, L., Lyu, X., Zhu, S., Zhao, Y., 2023a. Hydration inhibition and physical plugging to enhance shale stability using zwitterionic polymer/nanosilica composite. J. Mol. Liq. 387, 122642, 122642.

Xu, J., Wang, X., Chen, J., Ding, T., Xue, J., 2023b. Inhibition mechanism of cationic polyacrylamide on montmorillonite surface hydration: a molecular dynamics simulation study. Chem. Phys. 567, 111792, 111792.

Yang, L., Jiang, G., Yawei, S., Yang, X., 2017. Application of ionic liquid and polymeric ionic liquid as shale hydration inhibitors. Energy & Fuels 31, 4308–4317.

Yang, L., Yang, X., Tengda, W., Jiang, G., Luckham, P.F., Luckham, P.F., Li, X., Shi, H., Luo, J., 2019. Effect of alkyl chain length on shale hydration inhibitive performance of Vinylimidazolium-Based ionic liquids. Ind. Eng. Chem. Res. 58, 8565–8577.

Zhang, F., Sun, J., Chang, X., Xu, Z., Zhang, X., Huang, X., Liu, J., Lv, K., 2019a. A novel environment-friendly natural extract for inhibiting shale hydration. Energy & Fuels 33, 7118–7126.

Zhang, F., Sun, J., Chang, X, Xu, Z., Zhang, X., Huang, X., Liu, J., Lv, K., 2019b. A Novel Environment-Friendly Natural Extract for Inhibiting Shale Hydration. Energy & Fuels 33, 7118–7126. https://doi.org/10.1021/acs.energyfuels.9b01166.

Zhou, T., Yang, G., Xiao, Y., Baletabieke, B., Zhang, G., Jia, W., Huang, X., 2023. Development and mechanistic study of hydrophobic shale inhibitors for water-based drilling fluids. J. Dispersion Sci. Technol. 46 (3), 477–486.